frontiers | Frontiers in Energy Research

TYPE Original Research
PUBLISHED 07 November 2024
DOI 10.3389/fenrg.2024.1399371

OPEN ACCESS

EDITED BY
Sudhakar Babu Thanikanti,
Chaitanya Bharathi Institute of Technology, India

REVIEWED BY
Dong Ha,
Virginia Tech, United States
Sahil Tahiliani,
Applied Materials, United States

*CORRESPONDENCE
Godlove Suila Kuaban,
gskuaban@iitis.pl

RECEIVED 11 March 2024
ACCEPTED 04 October 2024
PUBLISHED 07 November 2024

CITATION
Kuaban GS, Czachórski T, Gelenbe E, Pecka P, Sharma S, Singh P, Nkemeni V and Czekalski P (2024) Energy performance of self-powered green IoT nodes.
Front. Energy Res. 12:1399371.
doi: 10.3389/fenrg.2024.1399371

Energy performance of self-powered green IoT nodes

Godlove Suila Kuaban[1]*, Tadeusz Czachórski[1], Erol Gelenbe[1], Piotr Pecka[1], Sapana Sharma[2], Pradeep Singh[2], Valery Nkemeni[3] and Piotr Czekalski[4]

[1]Institute of Theoretical and Applied Informatics, Polish Academy of Sciences (IITiS-PAN), Gliwice, Poland, [2]Department of Mathematics, Maharishi Markandeshwar Engineering College, Maharishi Markandeshwar (Deemed to be University), Haryana, India, [3]Laboratory of Electrical Engineering and Computing, Faculty of Engineering and Technology, University of Buea, Buea, Cameroon, [4]Faculty of Automatic Control, Electronic, and Informatics, Silesian University of Technology Gliwice, Gliwice, Poland

The widespread adoption of the Internet of Things (IoT) partly depends on the successful design and deployment of IoT nodes that can operate for several years without any service outage and the need to replace their energy storage systems (ESSs) (e.g., battery, capacitor, or supercapacitor) when all the stored energy is depleted or when the cycle life of the ESSs is reached. Replacing batteries in the case of large-scale IoT networks and nodes located in places that are hard to reach is very challenging and costly, requiring the design of IoT nodes that can operate for several years without the need for human intervention. One such example is the deployment of IoT nodes in large agricultural fields (for soil or crop monitoring) or a long-distance pipeline (for pipeline monitoring). In this paper, we investigated the practical implications of imposing energy-saving thresholds on the energy performance metrics of green IoT nodes. We propose an energy packet-based model for the evaluation of the energy performance of a green IoT node with the possibility of switching the node to energy-saving regimes on the fly when the energy content of the ESS reaches defined thresholds. Configuring single or multiple thresholds improves the energy performance of the node significantly (e.g., increases the lifetime of the node and reduces the probability of service outage and energy wastage), and the value of the threshold(s) should be carefully chosen. The energy performance of the IoT node can also be improved by dimensioning the energy harvesting system to ensure that the node operates for several years without running out of energy (e.g., maximizing the lifetime of the nodes and minimizing the probability of service outage and energy wastage).

KEYWORDS

energy performance, green IoT, energy packets, energy efficiency, energy thresholds, time-dependent analysis

1 Introduction

The widespread adoption of the Internet of Things (IoT) partly depends on the successful deployment of IoT nodes that can operate for several years without the need for battery replacement. In most IoT deployments, the IoT sensor/actuator nodes are powered by non-rechargeable batteries. A significant drawback of using non-rechargeable batteries is that the lifetime of the IoT network is limited by the finite energy capacity of their batteries (Ku et al. (2015)). As energy depleted from the battery is not being replenished, the energy stored

in the battery is eventually depleted, requiring the replacement of batteries, which is a costly operation and also very challenging in large-scale IoT networks and nodes located in locations that are hard to reach. For example, it is very challenging and costly to replace the batteries of IoT nodes deployed in large agricultural fields (for soil or crop monitoring) or a long-distance pipeline (for pipeline monitoring). Thus, there is a severe need to design and deploy IoT networks in such a way that the nodes can operate for several years before requiring battery replacements.

There is growing interest in the adoption of green IoT design as a viable strategy to increase the lifetime of IoT nodes (the time required to deplete all the energy stored in the energy storage system of an IoT node), reduce the carbon footprint of IoT networks, and ensure environmental sustainability of IoT deployments. Green IoT (Al-Ansi et al. (2021); Sadatdiynov et al. (2023); Alsharif et al. (2023a)) is an IoT design framework that seeks to minimize the energy consumption from the manufacturing and operation of IoT systems with the aim of minimizing the carbon footprint or pollutants (e.g., CO_2, electronic wastes, and other toxic substances) produced from the manufacturing, deployment, and operation of IoT systems including other IoT-related infrastructures (e.g., edge computing, core networks, cloud computing, and operation, provisioning, and maintenance systems).

Green IoT design involves the development of strategies to minimize energy consumption and the use of energy harvesters to harvest energy from ambient renewable energy sources to power IoT systems. Some green IoT design mechanisms to minimize energy consumption include duty cycling, reduction of packet size, transceiver optimization, energy-ware routing, energy-efficient sensing (e.g., adaptive sensing), reduction of protocol overhead, voltage and frequency control (Abdul-Qawy et al. (2020); Alsharif et al. (2023b)), energy-efficient hardware and software design (Albreem et al. (2021); Alsharif et al. (2023b)), green IoT communication technologies (BLE, RFID, NFC, Zigbee, LoRa, and Sigfox), green IoT architecture design (green cloud, fog, and virtualization) (Varjovi and Babaie (2020)), sustainable materials, and integration of renewable energy into IoT systems. In addition, the energy consumption of the IoT node can be reduced on the fly during its operation by throttling the speed of the processor clock, decreasing the operating voltage, or decreasing the transmission power (and the number of transmission operations).

The challenge in designing IoT nodes that can operate for several years without the need for battery replacement is the fact that the availability of ambient energy sources (e.g., light, wind, RF, heat, and vibration) is random and sporadic, and the energy consumed by the nodes varies slightly. An approach for dimensioning green IoT nodes without getting into the technical details of the energy harvesters, IoT nodes, and energy storage systems (ESSs) is to discretize energy into energy packets and apply well-known stochastic models such as Markov models. More details about the energy packet concept can be found in the study by Gelenbe (2011) and Gelenbe (2012) and Kuaban et al. (2023a), and we have also presented more details about it in the next section within the context of our proposed modelling framework.

A few studies (Gautam and Dharmaraja (2018); Jones et al. (2011); Tunc and Akar (2017); Miao et al. (2023)) were conducted to analyze the energy performance of green IoT networks with the possibility of reducing the energy consumption of the node on the fly when the energy content of the ESS goes below the defined energy thresholds. In the analysis presented in most of these works, a single energy threshold is considered. Most of these works mainly focus on performance metrics such as the lifetime of the node. However, there are other performance metrics, such as service outage probability, the mean energy content of the ESS, and the energy wastage probability. There is also a need for a more extensive investigation of the impact of the energy threshold on the energy performance metrics.

The main goal of this paper is to investigate the practical implications of imposing energy-saving thresholds on the energy performance metrics of green IoT nodes. We conduct steady-state and time-dependent analyses of the energy performance of a green IoT node, considering the impact of switching the node to more energy-efficient regimes when the defined threshold of the energy content of their ESS is reached. The main contributions of the paper include the following:

1. We propose an energy packet-based model for the evaluation of the energy performance of a green IoT node with the possibility of switching the node to more efficient regimes on the fly when the energy content of the ESS reaches defined thresholds.
2. We present an approach to determine the size of an energy packet or quantization step that can be used to discretize or quantize the energy flows (energy harvested, stored, and consumed) into energy packets. In this way, energy is treated as the flow of discrete energy units (the so-called energy packets) rather than continuous flows.
3. We propose a multi-threshold model of the ESS and evaluate the impact of the value and number of thresholds on the energy performance metrics such as the service outage probability (the probability that all the energy packets stored in the ESS are depleted), energy wastage probability (the probability that ESS is full and energy packets that arrive after this time instant are lost or wasted), the mean number of energy packets in the ESS, and the lifetime of the ESS.
4. We propose a novel Markov-based approach to model the performance of ESSs with time-dependent renewable energy sources (e.g., solar energy sources) similar to the approach proposed by Kuaban et al. (2024a,b) using diffusion approximation models. The model considers the accumulation of solar energy during the day, which is then consumed during the night when the solar energy harvester cannot harvest energy.

2 Model description

In this section, we describe the energy model of a self-powered green IoT node considered in this paper. We also describe the energy packet model of the node and then use it to describe the energy threshold-based model of the ESS, which is the main focus of this paper.

2.1 Energy model of the self-powered IoT node

Consider a typical self-powered IoT node that consists of an IoT sensor node, an energy harvesting system, and an ESS, as shown in Figure 1. Energy is harvested from ambient or external sources (e.g., solar, artificial light, radio frequency, and vibration) to power the sensor node directly. Any residual energy is stored in an ESS. The stored energy is used to power the sensor node when the energy harvester is not able to generate enough energy to meet the energy needs of the node due to unfavourable environmental conditions (e.g., during the night in the case of solar energy harvesters). When the sensor node is not performing sensing, computing, or processing operations, it is forced into the sleep mode, where it consumes negligible amounts of energy. Figure 2 shows a snapshot of the power profile of an IoT node consisting of two modes: sleep mode (when it is not performing sensing, computing, or communication functions) and active mode (when it wakes up to perform sensing, computing, or communication operations). From the power profile, the average power consumption of the node is given in Equation 1:

$$P_{node} = D \cdot P_{act} + (1 - D) \cdot P_{sleep}, \tag{1}$$

where the duty cycle ratio is given in Equation 2,

$$D = \frac{t_{act}}{t_{act} + t_{sleep}}. \tag{2}$$

where t_{act} is the time spent in the active mode and t_{sleep} is the time spent in the sleep mode. P_{act} is the power consumption of the node in the active mode and P_{sleep} is the power consumption of the node in the sleep mode. The energy consumed during the active mode is the sum of the energy consumed by the sensing, computing, communication units, and other auxiliary electronics components of the node during the active period.

The power profile in Figure 2 illustrates the characteristics of the IoT energy consumption model, which forms the basis of our energy packetization or quantization model in the following subsection. The power profile is obtained using a laboratory testbed that consists of two IoT nodes positioned 2 m apart along a high-pressure plastic pipe measuring 12 m in length and with a diameter of 25 mm. In order to optimize or minimize the energy consumption of the IoT nodes, the nodes are configured to perform distributed computing with Kalman filtering (by sharing the computing load), adaptive sensing (by using an energy-efficient but less accurate accelerometer sensor and an energy-hungry but more accurate accelerometer sensor), and duty cycling (forcing the node to enter sleep modes when it is idle).

Performing energy planning of self-powered IoT nodes requires an estimate of the energy demand, energy generation, and storage capacity to ensure a low probability of service outage and a long lifetime for the node. From the characterization of the energy harvesting system (e.g., solar cells, piezoelectric, RF, or thermoelectric energy harvester), the power profile can be obtained. An empirical power profile of a solar energy harvester for an IoT node is shown in the study by Kuzman et al. (2019), which consists of active periods of solar power generation (when there is enough solar radiation) and a period of no solar power generation (when there is insufficient solar radiation, notably during the night). From the energy consumption and generation profile, the mean energy produced and consumed can be estimated. The mean energy generated and consumed can be used to determine the number of energy packets produced and consumed per unit of time, as discussed in the next section.

2.2 The energy packet model of the node

In order to discretize or quantize energy into energy packets, the first step is to determine the quantization step, which, in our case, is the size of the energy packet. We consider an energy packet (in mWh or mAh) as a pulse of power or current which lasts for a defined time duration. Assuming that energy is consumed during active periods when the node wakes up to perform sensing, computing, or communication (and that a negligible amount of energy is consumed during the deep sleep period), the size of the energy packet can be considered to be $E_p = P_{act} \cdot t_{act}$. However, the quantization step can be set to any arbitrary value but must be kept consistent in the quantization of the energy harvesting, consumption, and storage processes, as in the study by Da Silva et al. (2017).

Let C_B (measured in mWh) represent the capacity of the ESS, which may be a battery or a supercapacitor. Then, the capacity of the ESS (in energy packets) is $B = C_B/E_p$; that is, the number of energy packets that can be stored in the ESS is B, and the energy states of the ESS are $\{0, 1, 2, \ldots, B\}$. We assume that the node wakes up only when triggered by a random event (e.g., leakage of fluids from a pipe in the case of a pipeline monitoring system). In this case, the energy drawn from the battery per time unit is scattered independently and uniformly in the sense of a Poison process (Kaj and Konané, 2016). The energy consumption process becomes $E_{node} = t_{act} \cdot P_{act} N_t^{(1/t_i)}$, where N_t^{μ} denotes a standard Poisson process on the half line with constant intensity μ. That is, energy is drawn from the battery in small jumps of energy $E_p = t_{act} \cdot P_{act}$, which occur interspaced by independent and exponentially distributed waiting times with expected value $t_i = t_{act} + t_{sleep}$. From the power consumption profile, the mean number of energy packets drawn from the ESS per time unit in the time interval $[0, \quad t_i]$ is

$$\mu = \frac{t_{act}}{t_{act} + t_{sleep}} \cdot \frac{P_{act}}{E_p}. \tag{3}$$

We consider an intermittent energy harvesting source (e.g., the presence of solar radiation, light, vibration, wind, RF radiation, and heat). For simplicity, we assume that the energy arrival times of the energy packets follow a Poisson process with rate λ_H (Ng et al., 2013; Wang et al., 2014). This assumption may be realistic in self-powered IoT nodes that stay in a deep sleep mode for a time that is exponentially distributed. They wake up to receive or transmit data packets, harvest wireless RF energy at the same time, and then return to the sleep mode. From the power generation profile of the energy harvester, the number of energy packets generated per time unit in the time interval $[0, \quad T]$ is as follows:

$$\lambda_H = \frac{1}{E_p \cdot T} \int_0^T P_H(\tau)\, d\tau. \tag{4}$$

Here, $P_H(t)$ is the output energy profile of the energy harvesting system. If the harvested energy is greater than the energy required to power the IoT node, the surplus is stored in the battery to be

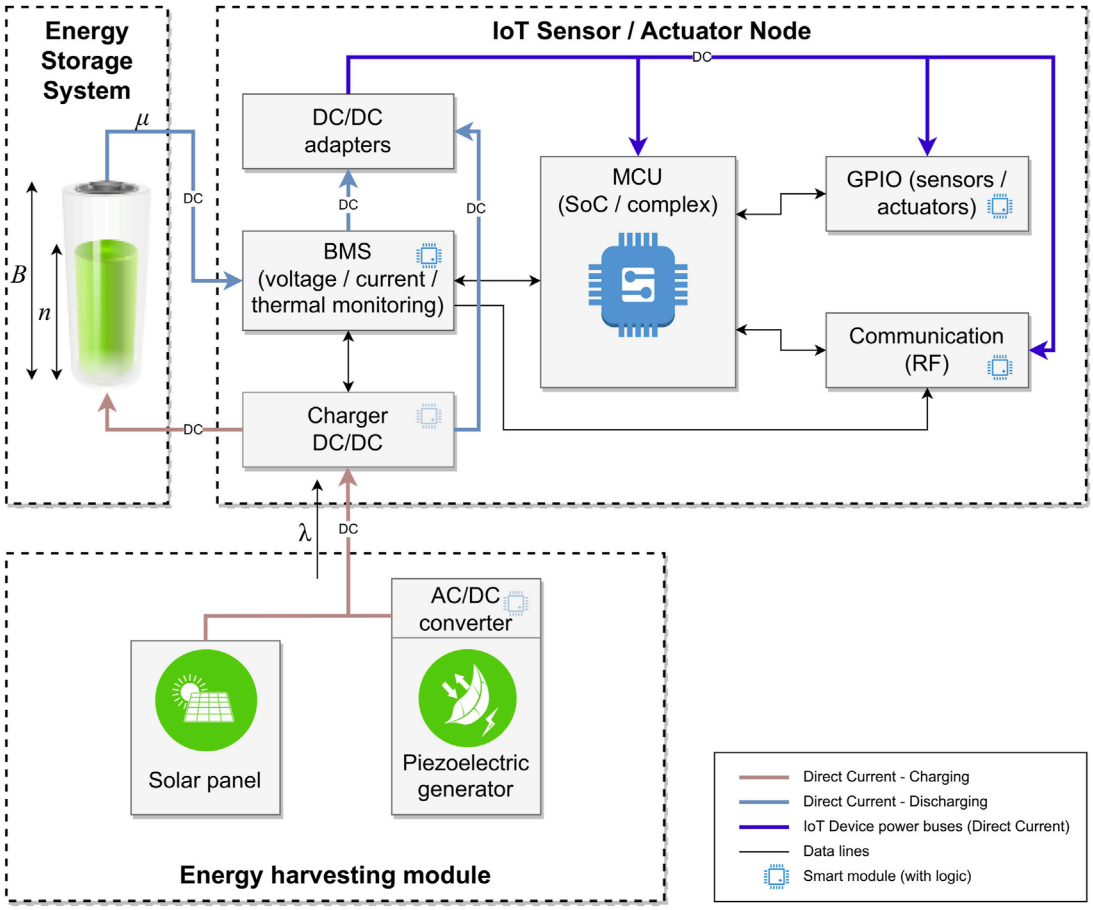

FIGURE 1
Architecture of a self-powered green IoT sensor node.

used when the node's needs are greater than the energy production. From the energy conservation principle and assuming that there is no energy leakage from the ESS, the mean number of energy packets delivered to the battery is $\lambda = \mu - \lambda_H$, which also follows a Poisson process. In this case, the process of delivering energy packets of the battery is also assumed to follow a Poisson process and from Equations 3, 4, the mean rate of delivering energy packets to the battery is $\lambda = \lambda_H - \mu$.

2.3 Markov model of an energy storage system with multiple energy thresholds

The ESS storage space is partitioned into m non-overlapping intervals called energy-saving regimes by introducing $m-1$ energy-saving thresholds (or barriers or switches). In the m^{th} interval (with the highest energy content), the IoT node is fully functional and performs all its functions typically. However, in the subsequent intervals, some of the functionalities of the node may be limited or disabled to save energy to prolong the lifetime of the device, making the node semi-functional. In the first interval (with the lowest energy content), most of the functionalities (computation and communication) of the nodes are significantly limited or disabled; that is, the node is non-functional. Therefore, the node's mean rate of energy consumption depends on the energy content of the energy storage system as shown in Equation 5:

$$\mu(n) = \begin{cases} \mu_1 & 0 < n \le K_1, \\ \mu_2 & K_1 < n \le K_2, \\ \mu_3 & K_2 < n \le K_3, \\ \cdots & \cdots, \\ \mu_m & K_m < n \le B. \end{cases} \tag{5}$$

By introducing energy thresholds and reducing energy consumption at the node as the energy content of the ESS goes below the various thresholds, the lifetime of the node can be increased. For specific IoT sensors, energy consumption can be reduced on the fly by throttling the speed of the processor clock, decreasing the operating voltage, or decreasing the transmission power. The drawback of forcing the node to enter into energy-saving modes is that it may degrade the quality of service of the nodes. This should only be considered when the energy stored in the ESS is below certain critical thresholds, and sacrificing some level of performance is acceptable. Energy modes for some IoT devices may include the following: run mode (CPU, flash, SRAM, and peripheral on), doze mode (CPU clock runs slower than peripheral on), idle mode (CPU

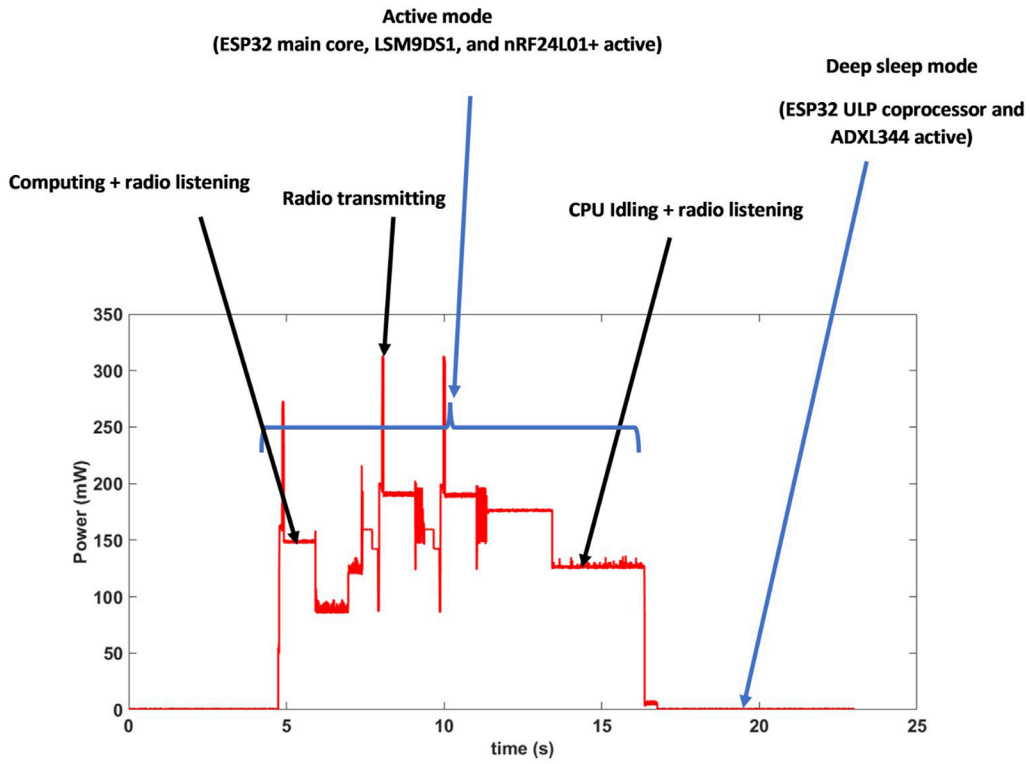

FIGURE 2
Snapshot of the power profile of an IoT node.

off, flash, SRAM, and peripheral on), sleep mode (CPU, flash, SRAM off, and peripheral on), and deep sleep mode (CPU, flash, SRAM, and peripheral off) (Evanchuk, 2024).

In the ESS model, we assume that energy is delivered and consumed by quantum (energy packets). The process resembles the behaviour of a queueing system. The energy packets are like customers, and the time it takes to consume one packet corresponds to the service time. The number of customers in the queueing system denotes the energy in the ESS. It allows us to make use of the existing queueing models. We model the dynamic changes in the number of energy packets in the ESS as an M/M(n)/1/B queueing Markov process $\{N(t)|t \geq 0\}$ such that $p(n,t) = \Pr\{N(t) = n\}$ is the probability of having n energy packets in the ESS. In the notation, based on the study by Kendall)53), it is a station with Poisson input, exponentially distributed service time, single server, and limited to B number of customers inside. M(n) underlines that the parameter μ of the time to consume an energy packet may depend on the queue length (number of energy packets in the ESS), $\mu = \mu(n)$. The model consists of a set of equations (see, e.g., Kleinrock (1975)), as follows:

$$\begin{aligned}
\frac{dp(0,t)}{dt} &= -\lambda p(0,t) + \mu(1)p(1,t), \\
\frac{dp(n,t)}{dt} &= -(\lambda + \mu_1)p(n,t) + \lambda p(n-1,t) + \mu(n)p(n+1,t), \\
&\qquad n = 1, \ldots B-1, \\
\frac{dp(B,t)}{dt} &= \lambda p(B-1,t) - \mu(B)p(B,t). \qquad (6)
\end{aligned}$$

This system has a well-known solution, both in transient and steady states, if the parameter μ does not depend on n, but in the case of $\mu(n)$, the solution is limited to a steady state when state probabilities do not depend on time. Therefore, in Section 3.2, we analyze its transient state in detail. The model can be extended to the case where the distributions between the time of arrival of energy packets and the distributions of the time of their consumption are not exponential but are a linear combination of exponentially distributed phases that can approximate any distribution. Many software tools adapt the parameters of such distributions to the actual measurement data (e.g., Asmussen et al. (1990) and Bause et al. (2010)), as well as tools to numerically solve the resulting Markov chain equations (e.g., Prism, Kwiatkowska et al. (2011), or our Olymp, Pecka et al. (2018)).

3 The energy performance analysis

The equations that are part of the set of Equation 6 are solved to determine the performance metrics such as the mean number of energy packets in the ESS, the probability that all the energy packets stored in the ESS are depleted, the probability that ESS is full and energy packets that arrive after the ESS is full are lost (energy wastage probability), and the density of the lifetime of the node. We perform both the steady-state and transient-state analyses of the performance of the ESS to provide more insights into the influence of the mean number of energy packets delivered to the ESS, the mean

energy consumption rate, and the energy threshold(s) on the energy performance of the node.

3.1 Steady-state analysis

In the steady state, when $\lim_{x\to\infty} p(n,t;n_0) = p(n)$, the differential equations above become linear equations which can be easily solved to derive the steady-state distribution of the number of energy packets in the ESS and the probability $p(0)$ of depleting all the energy packets stored in the ESS (probability that the ESS is empty). The steady-state distribution of the number of energy packets in the ESS is as follows (e.g., Kleinrock, 1975):

$$p(n) = p(0)\frac{\lambda^n}{\mu(1)\quad\cdots\quad\mu(n)}, \tag{7}$$

and taking normalization $\sum_{n=0}^{B} p(n) = 1$, the probability $p(0)$ of depleting all the energy packets stored in the ESS is as follows:

$$p(0) = \frac{1}{1+\sum_{n=1}^{B}\left\{\lambda^n / \prod_{i=0}^{n-1}\mu(i+1)\right\}}.$$

From the Equation 7 above, the steady-state probability $p(B)$ that the ESS is full can be derived. The energy storage space of the ESSs (e.g., battery or supercapacitor) for IoT nodes is very limited (especially for very small and mobile IoT nodes), and energy packets that arrive when the ESS is full are lost, resulting in undesirable energy wastage. In addition, when all the energy packets stored in the ESS are depleted, the node shuts down, interrupting the service provided by the node. Thus, the probability $p(0)$ is a critical performance metric and can be considered the service outage probability. In the case of a single threshold, K, there are two energy consumption regimes with $\mu(u) = \mu_1$ (for $n < K$) and $\mu(n) = \mu_2$ (for $n > K$), and the performance metrics are also a function of the energy threshold K.

3.2 Transient-state analysis

We present the transient-state analysis of the energy performance of the ESS with energy thresholds. The steady-state analysis assumes that the mean rate at which energy packets are delivered to the ESS and the mean rate at which energy packets are consumed from the ESS are constant. However, the mean number of energy packets harvested may vary within a 24-h day period and between various days and months. In the case of solar energy harvesters, sufficient energy is generated during the solar hour period of the day, and no energy is generated at night. There are also fluctuations within the day that may result in fluctuations in the mean number of energy packets harvested and the mean number of energy packets delivered to the ESS. These time-dependent changes in the number of energy packets harvested and delivered to the ESS make transient analysis of the dynamic changes in the energy content of the ESS interesting. In the transient-state analysis, the performance metrics considered in the previous section in the steady-state analysis become time-dependent.

Transient analysis of M/M/1/B was performed in the study by Tákacs (1962), Morse (1958), Sharma and Gupta (1982), and recently in the study by Massey et al. (2023). Here, we extend it to the case of M/M/(n)/1/B, that is, state-dependent parameters $\mu(n)$. The most straightforward approach is to consider Equation 6 in Laplace domain as shown in the set of equations in Equation 8.

$$\begin{aligned}
sP(0,s) - p(0,0) &= 1 - \lambda P(0,s) + \mu_1 P(1,s)\\
sP(n,s) - p(n,0) &= -\left[\lambda + \mu(n)\right]P(n,s) + \lambda P(n-1,s)\\
&\quad + \mu_1 P(n+1,s) \qquad 1 \le n < B\\
sP(B,s) - p(B,0) &= \lambda P(B-1,s) - \mu_B P(B,s) \qquad n = B.
\end{aligned} \tag{8}$$

Here,

$$\begin{aligned}
P(n,s) &= \mathcal{L}p(n,t) = \int_0^\infty e^{-st} p(n,t)\,dt \text{ and}\\
\mathcal{L}\left\{\frac{p(n,t)}{dt}\right\} &= sP(n,s) - p(n,0),
\end{aligned}$$

Solve the system Equation 8 for the values of s needed by the inversion algorithm, and then the originals of $P(n,s)$ are looked for numerically, for example, with the use of the Stehfest algorithm (Stehfest, 1970):

$$p(n,t) = \frac{\ln 2}{t}\sum_{i=1}^{N} V_i\, P\left(n, s = \frac{\ln 2}{t} i\right),$$

and

$$V_i = (-1)^{N/2+i}\sum_{k=\left\lfloor\frac{i+1}{2}\right\rfloor}^{\min(i,N/2)} \frac{k^{N/2+1}(2k)!}{(N/2-k)!k!(k-1)!(i-k)!(2k-i)!}.$$

In our numerical computations, we used $N = 20$.

However, we also present the explicit expressions for $P(n,s)$. Below, we do it for the case when the buffer is initially empty, $p(0,0) = 1$. Similarly, results can be obtained for a 'mirror' process that starts at B and ends at 0.

We assume that $\mu(n)$ takes m values specific for m zones, as defined in Equation 5. Starting from the equations in the first interval (e.g., $1 \le n \le K_1 - 1$),

$$\lambda\frac{P(n-1,s)}{P(n,s)} = \left[(s+\lambda+\mu_1) - \mu_1\frac{P(n+1,s)}{P(n,s)}\right]. \tag{9}$$

Dividing both sides of Equation 9 by μ_1, we get the following:

$$\frac{\lambda}{\mu_1}\frac{P(n-1,s)}{P(n,s)} = \left[\left(\frac{s}{\mu_1} + \frac{\lambda}{\mu_1} + 1\right) - \frac{P(n+1,s)}{P(n,s)}\right]. \tag{10}$$

From Equation 9,

$$\frac{P(n+1,s)}{P(n,s)} = \frac{\lambda}{\left[(s+\lambda+\mu_1) - \mu_1\frac{P(n+2,s)}{P(n+1,s)}\right]}. \tag{11}$$

Substituting (Equation 11) in (Equation 10), we get Equation 12:

$$\begin{aligned}
&\frac{\lambda}{\mu_1}\frac{P(n-1,s)}{P(n,s)}\\
&\quad = \left[\left(\frac{s}{\mu_1} + \frac{\lambda}{\mu_1} + 1\right) - \frac{\lambda}{\left[(s+\lambda+\mu_1) - \mu_1\frac{P(n+2,s)}{P(n+1,s)}\right]}\right],
\end{aligned} \tag{12}$$

which can be rearranged as follows:

$$\frac{\lambda}{\mu_1}\frac{P(n-1,s)}{P(n,s)} = \left[\left(\frac{s}{\mu_1}+\frac{\lambda}{\mu_1}+1\right) - \frac{\frac{\lambda}{\mu_1}}{\left[\left(\frac{s}{\mu_1}+\frac{\lambda}{\mu_1}+1\right) - \frac{P(n+2,s)}{P(n+1,s)}\right]}\right]. \quad (13)$$

The ratio $\frac{\lambda}{\mu_1}\frac{P(n-1,s)}{P(n,s)}$ in Equation 13 can be expressed as a hypergeometric series as follows:

$$\frac{\lambda}{\mu_1}\frac{P(n-1,s)}{P(n,s)} = \left[\left(\frac{s}{\mu_1}+\frac{\lambda}{\mu_1}+1\right) - \frac{\frac{\lambda}{\mu_1}}{\left[\left(\frac{s}{\mu_1}+\frac{\lambda}{\mu_1}+1\right) - \frac{\frac{\lambda}{\mu_1}}{\left(\frac{s}{\mu_1}+\frac{\lambda}{\mu_1}+1\right)-\cdots}\right]}\right]. \quad (14)$$

We apply the concepts of hypergeometric functions (Lorentzen and Waadeland, 1992) and finite continued fractions (Waadeland and Lorentzen, 2008; Ikenaga, 2022, accessed on 12 February, 2022) to simplify the hypergeometric series in Equation 14. Let

$$x = \left[\left(\frac{s}{\mu_1}+\frac{\lambda}{\mu_1}+1\right) - \frac{\frac{\lambda}{\mu_1}}{\left[\left(\frac{s}{\mu_1}+\frac{\lambda}{\mu_1}+1\right) - \frac{\frac{\lambda}{\mu_1}}{\left(\frac{s}{\mu_1}+\frac{\lambda}{\mu_1}+1\right)-\cdots}\right]}\right],$$

which can also be expressed as follows:

$$x = (a+b) - \frac{b}{(a+b) - \frac{b}{(a+b)-\frac{b}{(a+b)-\cdots}}},$$

where $a = \frac{s}{\mu_1}+1$ and $b = \frac{\lambda}{\mu_1}$. As x contains a copy of itself as the bottom of the first fraction, it can be expressed as follows:

$$x = (a+b) - \frac{b}{x}. \quad (15)$$

The roots of Equation 15 are as follows:

$$x = \frac{(a+b) \pm \sqrt{(a+b)^2 - 4b}}{2}.$$

As the fraction is positive, we take the positive root of Equation 16,

$$x = \frac{(a+b) + \sqrt{(a+b)^2 - 4b}}{2}. \quad (16)$$

From Equations 14, 16

$$P(n,s) = \frac{2b}{(a+b)+\sqrt{(a+b)^2-4b}}P(n-1,s). \quad (17)$$

Therefore, for $1 \le n < K_1$, the transient state probabilities $P(n,s)$ are derived from Equation 17

$$P(n,s) = \left(\frac{\lambda}{\mu_1}\frac{1}{x}\right)^n, \quad (18)$$

where

$$x = \frac{s+\lambda+\mu_1+\sqrt{(s+\lambda+\mu_1)^2-4\lambda\mu_1}}{2\mu_1}.$$

Applying the above solution in Equation 18 iteratively for all intervals, we obtain the transient state probabilities are given in Equations 19–26:

$$P(n,s) = \begin{cases} \left(\frac{\lambda}{\mu_1}\frac{1}{\alpha_1(s)}\right)^n P(0,s), & 1 \le n \le K_1, \\ \left(\frac{\lambda}{\mu_2}\frac{1}{\alpha_2(s)}\right)^n P(0,s), & K_1 < n \le K_2, \\ \left(\frac{\lambda}{\mu_3}\frac{1}{\alpha_3(s)}\right)^n P(0,s), & K_2 < n \le K_3, \\ \cdots & \cdots, \\ \left(\frac{\lambda}{\mu_{m-1}}\frac{1}{\alpha_{m-1}(s)}\right)^n P(0,s), & K_{m-2} < n \le K_{m-1}, \\ \left(\frac{\lambda}{\mu_m}\frac{1}{\alpha_m(s)}\right)^n P(0,s), & K_{m-1} < n \le B-1. \end{cases} \quad (19)$$

where

$$\alpha_i(s) = \frac{s+\lambda+\mu_i+\sqrt{(s+\lambda+\mu_i)^2-4\lambda\mu_i}}{2\mu_i}, \qquad i = 1,2,3,\cdots m.$$

From first Equation 8,

$$(s+\lambda)P(0,s) = 1+\mu_1 P(1,s),$$

we obtain $P(0,s)$.

$$P(0,s) = \frac{(a+b)+\sqrt{(a+b)^2-4b}}{(s+\lambda)\left[(a+b)+\sqrt{(a+b)^2-4b}\right]-2\lambda}, \quad (20)$$

Equation 20 can be rearranged to obtain the transient probability of depleting all the energy packets stored in the ESS given in Equation 21:

$$P(0,s) = \frac{s+\lambda+\mu_1+\sqrt{(s+\lambda+\mu_1)^2-4\lambda\mu_1}}{(s+\lambda)\left\{s+\lambda+\mu_1+\sqrt{(s+\lambda+\mu_1)^2-4\lambda\mu_1}\right\}-2\lambda\mu_1}. \quad (21)$$

From last Equation 8,

$$(s+\mu_m)P(B,s) = \lambda P(B-1,s),$$

and the transient proability that the ESS is charged to its full capacity (and additional incoming energy packets are lost), $P(B,S)$ is given in Equation 22:

$$P(B,s) = \frac{\lambda}{s+\mu_m}\left(\frac{\lambda}{\mu_m}\frac{1}{\alpha_m(s)}\right)^{B-1}P(0,s). \quad (22)$$

We remind that in the case of an M/M/1/B model, the transient solutions obtained in Sharma and Gupta (1982) for the same initial condition $p(0,0) = 1$ and $p(n,0) = 0$, $n = 1,\ldots B$ is present in is present in Equation 23

$$P(n,s) = \frac{(\alpha\beta)^n\left[\alpha^{B-n+1}-\beta^{B-n+1}\right] - (\alpha\beta)^{n+1}\left[\alpha^{B-n}-\beta^{B-n}\right]}{s\left[\alpha^{B+1}-\beta^{B+1}\right]}, \quad (23)$$

where

$$\alpha(s) = \frac{s+\lambda+\mu+\sqrt{(s+\lambda+\mu)^2-4\lambda\mu}}{2\mu},$$

and

$$\beta(s) = \frac{s+\lambda+\mu-\sqrt{(s+\lambda+\mu)^2-4\lambda\mu}}{2\mu}.$$

Similarly,

$$P(0,s) = \frac{\left[\alpha^{B+1}-\beta^{B+1}\right]-(\alpha\beta)\left[\alpha^{B}-\beta^{B}\right]}{s\left[\alpha^{B+1}-\beta^{B+1}\right]}, \quad (24)$$

and

$$P(B,s) = \frac{(\alpha\beta)^{B}\left[\alpha-\beta\right]}{s\left[\alpha^{B+1}-\beta^{B+1}\right]}. \quad (25)$$

For very large values of B, the transient solution reduces to an M/M/1 model as follows:

$$\lim_{B\to\infty} P(n,s) = \frac{(1-\beta)\varrho^{n}}{s\alpha^{n}}, \quad (26)$$

where $\varrho = \lambda/\mu$ is the energy supply to demand ratio.

For other initial conditions, the system of Equation 8 is solved numerically.

The mean number of energy packets in the ESS at time t is

$$E[N(t)] = \sum_{n=0}^{B} np(n.t). \quad (27)$$

The Laplace transforms above can be inverted numerically using the Stehfest algorithm to obtain $p(n,t)$, from which time-dependent performance metrics such as the service outage probability $p(0,t)$, energy wastage probability $p(B,t)$, and the mean number of energy packets in the ESS $E[N(t)]$ can be obtained.

3.3 Modelling the lifetime of the IoT node

We investigate the impact of the threshold energy management policy on the device's lifetime. The objective of introducing the adaptive threshold (or imposing the energy-saving regimes) is to increase the device's lifetime. The device's lifetime is the time required to deplete all the energy packets stored in the ESS (Kuaban et al., 2023b; Czachórski et al., 2022). We model the device's lifetime as the first passage time of the M/M(n)/1/B model from any starting state to $n = 0$. The density of the first passage time, $\gamma_{i,0}(t)$, of the process that starts at $n = i$ and is absorbed at $n = 0$ can be obtained numerically by solving the proposed M/M(n)/1/B model.

We compute the first passage time from B to zero of the proposed M/M/(n)/1/B model by making state zero the absorbing one, that is, modifying the first equation of the system (6) to the following form:

$$\frac{dp(0,t)}{dt} = \mu(1)p(1,t).$$

If the $p(1,t)$ is computed for the chain initiated from state B, the intensity of entering state 0 in the equation above is the density of the first passage time from B to 0,

$$\gamma_{B,0}(t) = \mu(1)p(1,t). \quad (28)$$

Similarly, to model the first passage time from 0 to B (the time required to charge the ESS to its full capacity), we make B the absorbing state and compute $p(B-1,t)\lambda$ in the chain initiated at state 0.

$$\gamma_{0,B}(t) = \lambda p(B-1,t). \quad (29)$$

The performance metrics $\gamma_{B,0}$ (lifetime of the node) and $\gamma_{0,B}$ expressed in Equation 28 and 0; B expressed in Equation 29 can be obtained numerically using a Markov solver developed in Pecka et al. (2018).

4 Numerical results

In the numerical results presented, we consider a battery with a charge rating $Q = 2100$ mAh, depth of discharge $DoD = 70\%$, and voltage $v = 3.7$ volts. The energy capacity of the battery is $C_B = 2100^{*}0.7^{*}3.7 = 5439$ mWh. We assume that the quantization step (size of an energy packet) is $E_p = 54.39$ mWh, and the capacity of the battery in the energy packets (maximum number of packets that can be stored in the battery) is $B = 5439/54.39 = 100$ energy packets. Assuming that the mean energy delivered to the battery is 108.78 mWh, then the mean number of packets delivered to the battery per hour is $\lambda = 108.78/54.39 = 2$ energy packets per hour. Similarly, the mean number of energy packets consumed per hour is obtained. For each numerical example, we provide the values of the various parameters under the figure.

4.1 Energy performance of an IoT node with a non-solar renewable energy source

The steady-state and transient-state analyses presented in Section 3 above are more applicable to non-solar energy sources. That is, energy sources that can produce energy both in the day and in the night (e.g., RF, vibration, and wind). Figures 3–6 present the results obtained using the analytical models presented in the previous section.

Figure 3 presents the changes of the service outage probability, $p(0,t)$, as a function of time until attaining a steady state. The results compare two cases: one with a threshold and the other without a threshold. The introduction of a threshold significantly reduces the probability of service outage, $p(0,t)$.

Figure 4 illustrates the above solution in the case where the battery volume is $B = 100$ energy units. The only threshold is placed at $K = 40$, the consumption rates are $\mu(n) = \mu_1 = 3$ energy units per time unit, $n = 1,\ldots K$; if $\mu(n) = \mu_2 = 5$ energy units per time unit, $n = 41\ldots B$. Depending on the value of harvesting rate λ, the probability mass of $p(n)$ is concentrating close to 0 ($\lambda < \mu_1$), close to B ($\lambda > \mu_2$), or around K ($\mu_1 < \lambda < \mu_2$). If $\lambda = \mu_1$. The distribution does not change in the corresponding interval or $\lambda = \mu_2$.

Figures 5, 6 display the density of the lifetime of the IoT node $\gamma_{B,0}(t)$ for various values of the threshold $K = 20, 40, 60$ and various values of $\mu_1 = 2.5, 3, 4$; $\mu_2 = 5$ is not changing. The densities are compared with the same density when there is no threshold, and the unique rate is $\mu = 5$. The impact of the energy saving of the threshold K and reduced consumption rate μ_1 is essential. It influences not only the mean time to depletion but also the variance of the distribution.

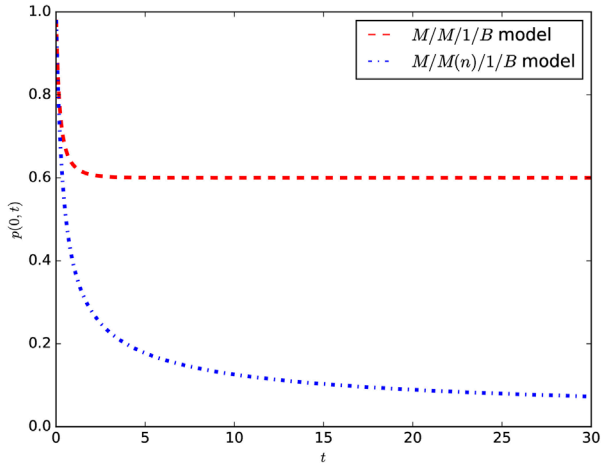

FIGURE 3
Comparison of the transient probability of service outage $p(0,t)$ from the M/M/1/B and M/M(n)/1/B for $\mu_1 = 2$, $\mu_2 = 5$, $\lambda = 2$, $K = 40$, and $B = 100$.

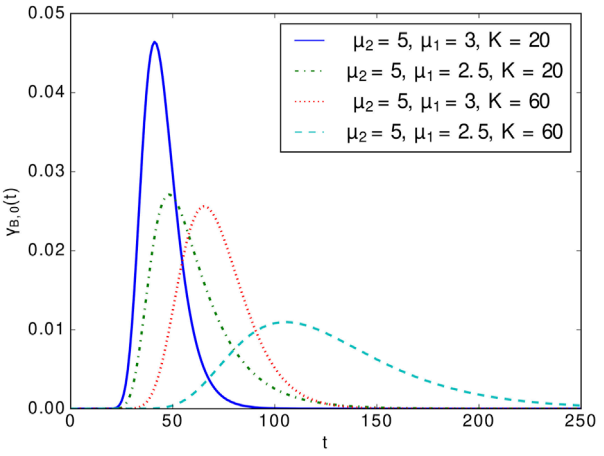

FIGURE 5
Influence of the proposed energy-saving threshold policy on the density of the lifetime of the IoT node $\gamma_{B,0}(t)$ for $K = 20, 60$, $\mu_2 = 5$, $\lambda = 2$, and $B = 100$.

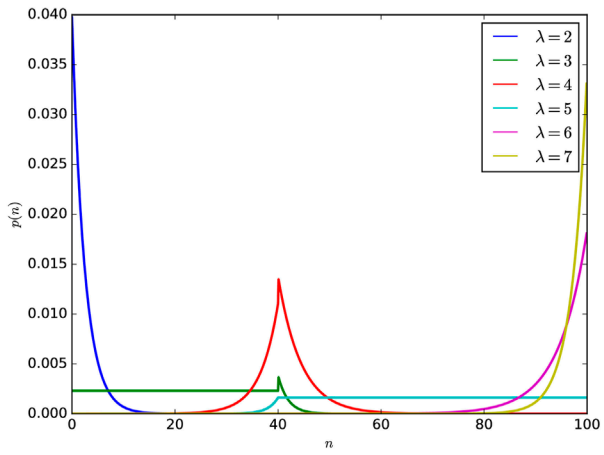

FIGURE 4
Influence of λ on the probability of having n energy packets in the battery for $\mu_1 = 3$, $\mu_2 = 5$, $B = 100$, and $K = 40$.

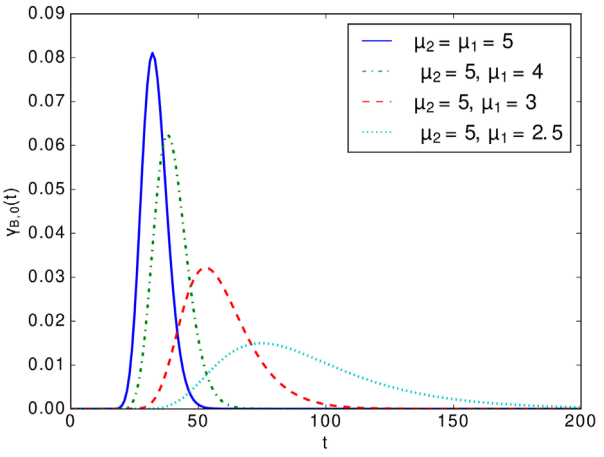

FIGURE 6
Influence of μ_1 on the density of the lifetime of the IoT node $\gamma_{B,0}(t)$ for $\mu_2 = 5$, $\lambda = 2$, $B = 100$, and $K = 40$.

4.2 Energy performance of an IoT node with a solar energy source

The energy produced by non-solar energy sources is relatively small and may be insufficient for some energy-hungry IoT nodes. A scalable approach to generate sufficient energy to power an IoT node is the use of solar energy. However, solar energy sources produce energy during the day and not during the night; that is, when energy is equally consumed. Thus, the analysis presented in Section 3 is not sufficient to analyze ESSs that are supplied by energy from solar energy sources.

As solar energy sources generate energy during the day, part of which is used to supply the node and the residue is stored to be consumed during the night, we propose an approach that takes into consideration the day and night cycles. We assume the interleaving of day and night periods of constant duration T_d and T_n; $T_d + T_n =$ 24 hours. That is, the ESS is charged during the day for a duration of T_d and discharged during the night for a duration of T_n (e.g., $T_d = T_n = 12$).

In this case, the performance metrics are obtained by numerically solving differential Equation 6 considering various initial conditions. During the day, the ESS is charged with a mean rate of $\lambda = \lambda_H - \mu(n)$, and during night, $\lambda = 0$ and the ESS is discharged at a mean rate of $\mu(n)$. The energy distribution at the end of a day makes the initial condition for the next night's solution, and *vice versa*. A few figures below present the numerical solutions for several consecutive night and day periods until we observe a repetitive behaviour of the ESS, independent of its state at the very beginning. In the 24-h cycle, we assume an equal day and night duration of 12 h. It, of course, may be easily changed.

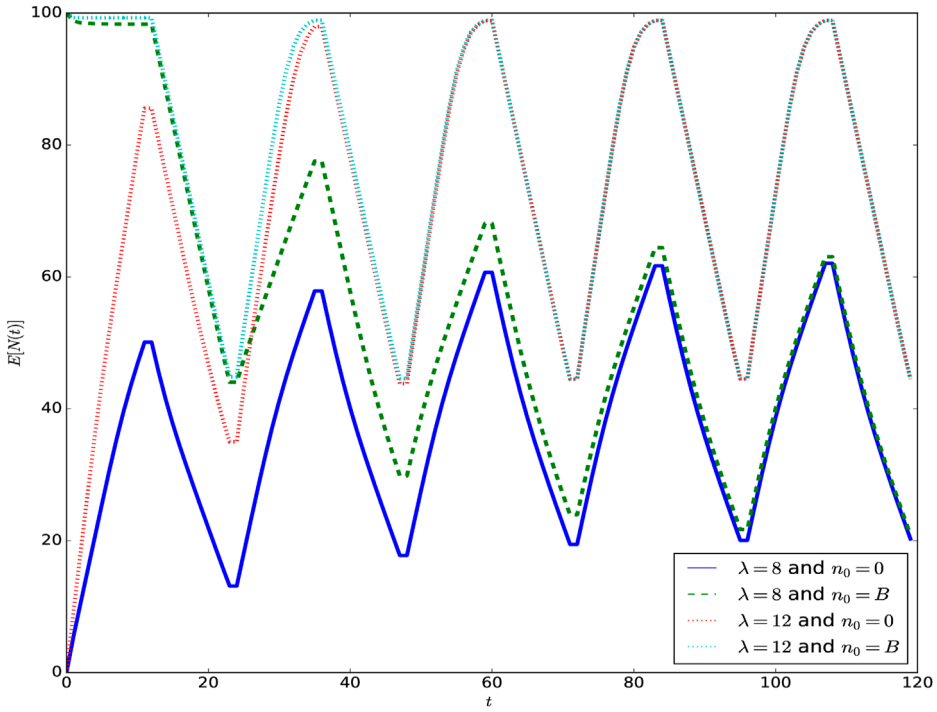

FIGURE 7
Dynamic evolution of the mean number of energy packets in the ESS, $E[N(t)]$, considering the cases with initial conditions $n_0 = 0$ (starting zero EPs in the ESS) and $n_0 = B$ (starting with B EPs in the ESS), $K = 40$.

Figure 7 presents the changes of the mean number of energy packets $E[N(t)]$, both for the primarily empty ($n_0 = 0$) and full ($n_0 = B$) ESS in case of two input flows $\lambda = 8$, $\lambda = 12$. After several periods, the influence of the initial value is not visible. The transient mean number of energy packets in the ESS is obtained using Equation 27.

Figure 8 refers to a case when the input rate is insufficient to maintain the performance of the node: in two cycles, the content of the initially full ESS goes down so that charging during the day is not sufficient to ensure continuous operation of the device. Two scenarios are considered: without threshold ($K = 0$) and with one threshold ($K = 40$). The flow is too weak to ensure good performance of the ESS even with the threshold; however, its presence increases the node's availability (when all the stored EPs are consumed).

Figure 9 illustrates the impact of the threshold position, $K = 20, 40, 80$, in case when the input rate is relatively high ($\lambda = 8$). The earlier the device enters into the energy efficient regime, the higher the number of EPs stored during the cycle.

Figure 10 shows the influence of input rate λ for a given threshold ($K = 40$) on the mean energy content during nights and days. $\lambda = 8, 12$ provide a safe energy reserve over the entire operating cycle, whereas lambda = 4 no longer ensures continuous operation. However, we should remember that the above curves refer to average energy values; analysis of the probability of a battery being empty or full as a function of time gives us more specific information.

In Figure 11, the probability of service outage, $p(0, t)$, is presented if, at the beginning, the ESS is full and the energy input rate is insufficient $\lambda = 4$. During the second night, the probability of complete depletion mounts sharply, and putting the threshold at $K = 40$ does not sufficiently improve the situation.

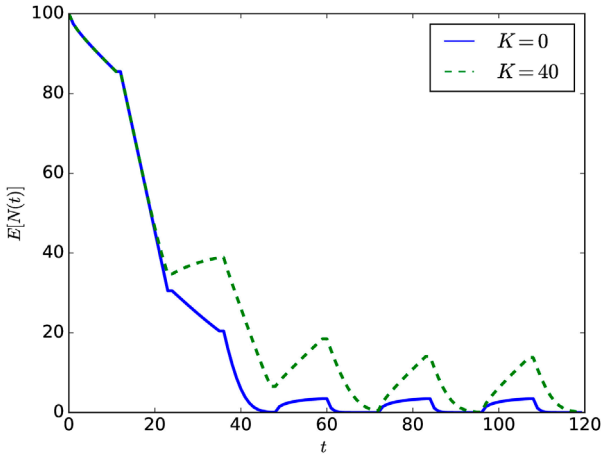

FIGURE 8
Dynamic evolution of the mean number of energy packets in the ESS, $E[N(t)]$, considering the case without threshold ($K = 0$) and the case with threshold ($K = 40$), $\lambda = 4$.

Figures 12, 13 refer to the time-varying probability that the battery is fully charged and further energy packets delivered are lost. In the first figure, in the presence of input rate $\lambda = 8$, we observe how lowering the threshold from position $K = 80$ to $K = 40$ reduces the probability of having a full ESS. In the second figure, we see the impact of increasing the input rate on the probability $p(B, t)$ for a

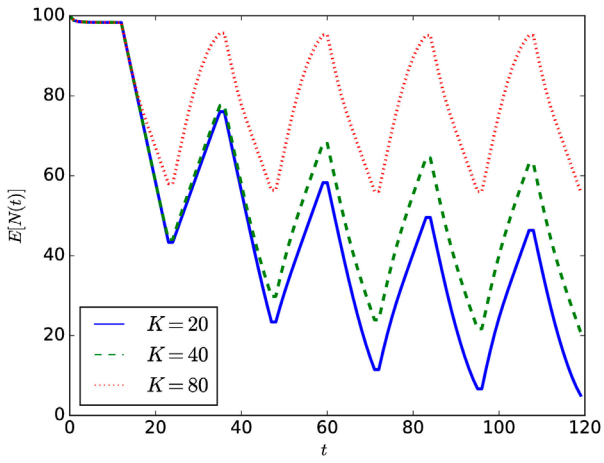

FIGURE 9
Influence of the energy threshold K on the dynamic evolution of the mean number of energy packets in the ESS $E[N(t)]$ for $\lambda = 8$.

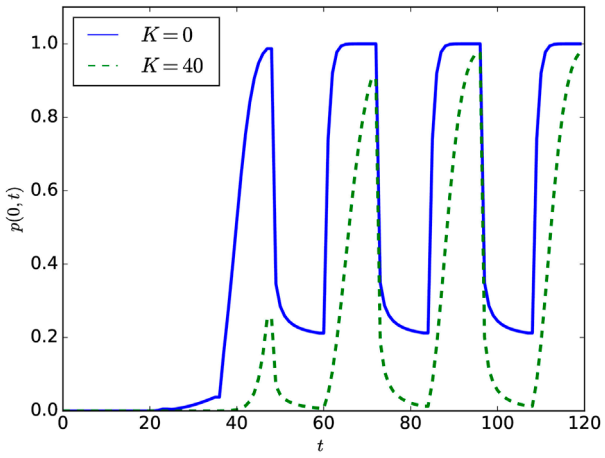

FIGURE 11
Dynamic evolution of the probability of service outage, $p(0,t)$, considering the case without threshold ($K = 0$) and the case with threshold ($K = 40$), $\lambda = 4$.

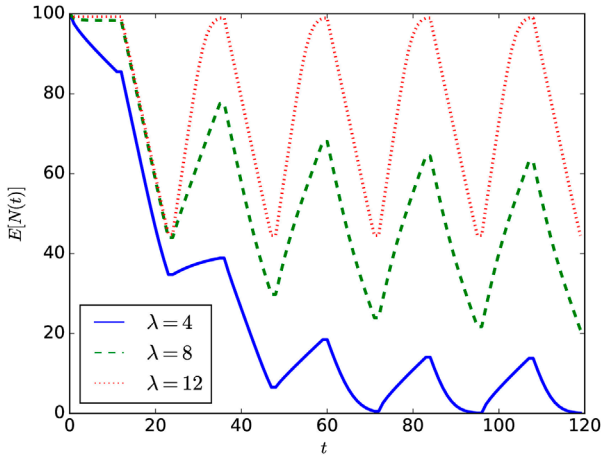

FIGURE 10
Influence of the mean charging rate λ on the dynamic evolution of the mean number of energy packets in the ESS $E[N(t)]$ for $K = 40$.

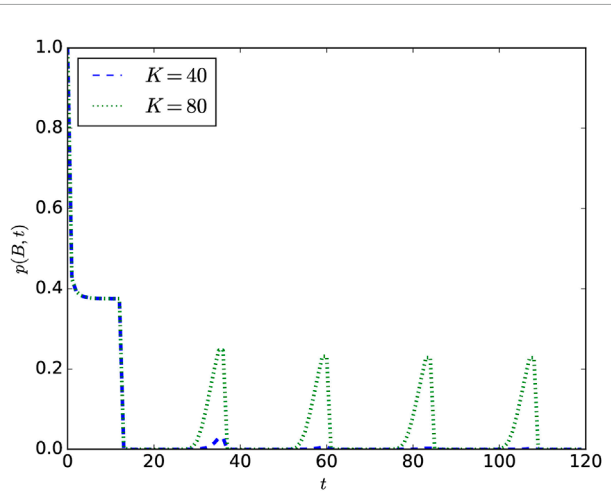

FIGURE 12
Influence of the energy threshold K on the probability of energy wastage, $p(B,t)$, for $\lambda = 8$.

fixed value $K = 40$ of threshold. Only for the highest value $\lambda = 12$, the probability of fully charged ESS at the end of the day is significant.

Finally, Figures 14, 15 refer to the lifetime of the IoT node showing the density $\gamma_{B,0}(t)$ of the first passage time from B to 0. The flow $\lambda = 4$ is insufficient to maintain the uninterrupted work of the ESS. With the threshold $K = 40$, the working time is longer and may last several periods; we see how nights and days shape the curve of the density. The second figure displays the same curves on logarithmic scale to demonstrate that the model is able to predict very weak probabilities.

5 Conclusion

In this paper, we have investigated the practical implications of imposing energy-saving thresholds on the energy performance metrics of green IoT nodes. We conducted steady-state and time-dependent analyses of the proposed energy packet-based model of the node, which consider the impact of switching the node to more energy-efficient regimes when the defined threshold of the energy content of the ESS is reached. We conducted numerical experiments to gain more insight into the extent to which the imposed energy threshold improves the energy performance of the green IoT node. We observed that configuring single or multiple thresholds improves the energy performance of the node significantly (e.g., increased lifetime of the node and reduced probability of service outage and energy wastage), and the value of the threshold(s) should be carefully chosen. In addition, the energy performance of the node can be improved by implementing energy-saving mechanisms to reduce the energy consumption rate of the node and to dimension the energy harvester in such a way that it harvests sufficient energy to meet the

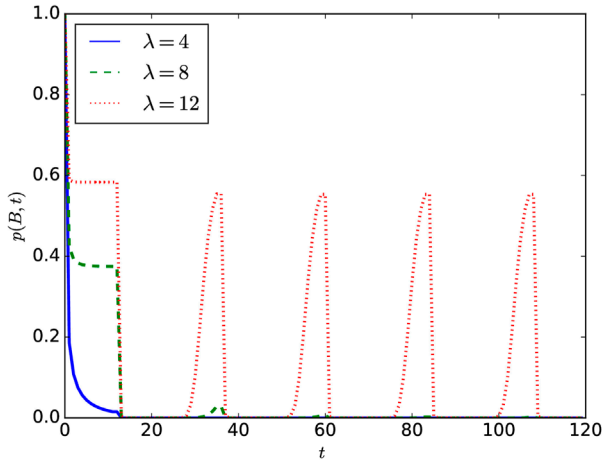

FIGURE 13
Influence of the mean charging rate λ on the probability of energy wastage, $p(B,t)$, for $K = 40$.

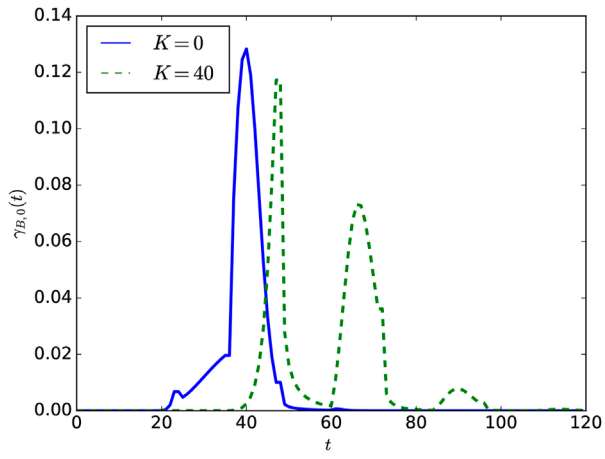

FIGURE 14
Density of the lifetime of the node, $\gamma_{B,0}(t)$, considering the case without threshold ($K = 0$) and the case with threshold ($K = 40$), $\lambda = 4$.

needs of the node during the day and store sufficient energy that can sustain the node throughout the night.

Data availability statement

The original contributions presented in the study are included in the article/supplementary material, further enquiries can be directed to the corresponding author.

Author contributions

GK: Conceptualization, Formal Analysis, Investigation, Methodology, Software, Validation, Visualization, Writing–original draft, Writing–review and editing. TC: Conceptualization, Supervision, Writing–original draft. EG: Conceptualization, Supervision, Writing–original draft. PP: Investigation, Software, Writing–review and editing. SS: Formal Analysis, Writing–review and editing. PS: Formal Analysis, Writing–review and editing. VN: Writing–original draft. PC: Conceptualization, Visualization, Writing–review and editing.

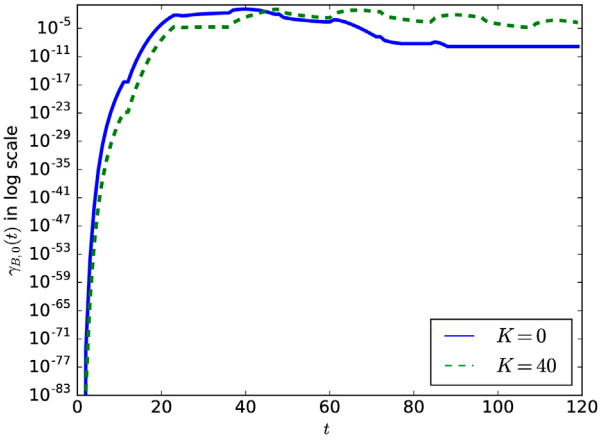

FIGURE 15
Density of the lifetime of the node, $\gamma_{B,0}(t)$ (in log scale), considering the case without threshold ($K = 0$) and the case with threshold ($K = 40$), $\lambda = 4$.

Funding

The author(s) declare that financial support was received for the research, authorship, and/or publication of this article. This paper was partially supported by the Reactive Too project that has received funding from the European Unions Horizon 2020 Research, Innovation and Staff Exchange Programme under the Marie Skodowska-Curie Action (Grant Agreement No871163); the Department of Graphics, Computer Vision and Digital Systems, under statute research project (Rau6, 2024), Silesian University of Technology (Gliwice, Poland); and the international project co-financed by the program of the Minister of Science and Higher Education entitled "PMW" in the years 2021–2025; contract no. 5169/H2020/2020/2.

Conflict of interest

The authors declare that the research was conducted in the absence of any commercial or financial relationships that could be construed as a potential conflict of interest.

Publisher's note

All claims expressed in this article are solely those of the authors and do not necessarily represent those of their affiliated

organizations, or those of the publisher, the editors, and the reviewers. Any product that may be evaluated in this article, or claim that may be made by its manufacturer, is not guaranteed or endorsed by the publisher.

References

Abdul-Qawy, A. S. H., Almurisi, N. M. S., and Tadisetty, S. (2020). Classification of energy saving techniques for iot-based heterogeneous wireless nodes. *Procedia Comput. Sci.* 171, 2590–2599. doi:10.1016/j.procs.2020.04.281

Al-Ansi, A., Al-Ansi, A. M., Muthanna, A., Elgendy, I. A., and Koucheryavy, A. (2021). Survey on intelligence edge computing in 6g: characteristics, challenges, potential use cases, and market drivers. *Future Internet* 13, 118. doi:10.3390/fi13050118

Albreem, M. A., Sheikh, A. M., Alsharif, M. H., Jusoh, M., and Yasin, M. N. M. (2021). Green internet of things (giot): applications, practices, awareness, and challenges. *IEEE Access* 9, 38833–38858. doi:10.1109/access.2021.3061697

Alsharif, M. H., Jahid, A., Kelechi, A. H., and Kannadasan, R. (2023a). Green iot: a review and future research directions. *Symmetry* 15, 757. doi:10.3390/sym15030757

Alsharif, M. H., Jahid, A., Kelechi, A. H., and Kannadasan, R. (2023b). Green iot: a review and future research directions. *Symmetry* 15, 757. doi:10.3390/sym15030757

Asmussen, S., Nerman, O., and Olsson, M. (1990). Fitting phase-type distributions via the em algorithm. *Scand. J. Statistics* 23, 419–441.

Bause, F., Buchholz, P., and Kriege, J. (2010). "Profido - the processes fitting toolkit dortmund," in *proc. of the 7th international conference on quantitative evaluation of systems* (IEEE Computer Society), 96. doi:10.1109/qest.2010.20

Czachórski, T., Gelenbe, E., and Kuaban, G. S. (2022). "Modelling energy changes in the energy harvesting battery of an iot device," in *Proceedings of the 2022 30th international symposium on modeling, analysis, and simulation of computer and telecommunication systems (MASCOTS)* (Nice, France: IEEE), 81–88. doi:10.1109/MASCOTS56607.2022.00019

Da Silva, A. P. C., Renga, D., Meo, M., and Marsan, M. A. (2017). The impact of quantization on the design of solar power systems for cellular base stations. *IEEE Trans. Green Commun. Netw.* 2, 260–274.

[Dataset] Evanchuk, E. (2024). Meeting power demand with energy harvesting in iot sensor nodes. Available at: https://www.digikey.pl/pl/articles/meeting-power-demand-with-energy-harvesting-in-iot-sensor-nodes (accessed on august, 2024).

Gautam, A., and Dharmaraja, S. (2018). An analytical model driven by fluid queue for battery life time of a user equipment in LTE-A networks. *Phys. Commun.* 30, 213–219. doi:10.1016/j.phycom.2018.08.004

Gelenbe, E. (2011). "Energy packet networks: ict based energy allocation and storage," in *International conference on green communications and networking* (Springer), 186–195.

Gelenbe, E. (2012). "Energy packet networks: adaptive energy management for the cloud," in *CloudCP'12: proceedings of the 2nd international workshop on cloud computing platforms* (ACM), 1–5. doi:10.1145/2168697.2168698

[Dataset] Ikenaga, B. (2022). Finite continued fractions. Available at: https://sites.millersville.edu/bikenaga/number-theory/finite-continued-fractions/finite-continued-fractions.html (accessed on February 12, 2022).

Jones, G. L., Harrison, P. G., Harder, U., and Field, T. (2011). "Fluid queue models of battery life," in *Proceeding of the 2011 IEEE 19th annual international symposium on modelling, analysis, and simulation of computer and telecommunication systems* (IEEE), 278–285. doi:10.1109/MASCOTS.2011.61

Kaj, I., and Konané, V. (2016). Modeling battery cells under discharge using kinetic and stochastic battery models. *Appl. Math. Model.* 40, 7901–7915. doi:10.1016/j.apm.2016.03.049

Kendall, D. G. (1953). Stochastic processes occurring in the theory of queues and their analysis by the method of the imbedded Markov chain. *Ann. Math. Statistics* 24, 338–354. doi:10.1214/aoms/1177728975

Kleinrock, L. (1975). *Queueing systems vol. 1: theory*. John Wiley and Sons.

Ku, M.-L., Chen, Y., and Liu, K. R. (2015). Data-driven stochastic models and policies for energy harvesting sensor communications. *IEEE J. Sel. Areas Commun.* 33, 1–1520. doi:10.1109/jsac.2015.2391651

Kuaban, G. S., Czachórski, T., Gelenbe, E., Sharma, S., and Czekalski, P. (2023a). "A markov model for a self-powered green iot device with state-dependent energy consumption," in *2023 4th international conference on communications, information, electronic and energy systems (CIEES)*, 1–7. doi:10.1109/CIEES58940.2023.10378778

Kuaban, G. S., Gelenbe, E., Czachórski, T., and Czekalki, P. (2024a). "Modelling the energy performance of off-grid sustainable green cellular base stations," in *Proceedings of the 2023 31th international symposium on modeling, analysis, and simulation of computer and telecommunication systems (MASCOTS)* (New York, USA: IEEE). Stony brooks.

Kuaban, G. S., Gelenbe, E., Czachórski, T., Czekalski, P., and Nkemeni, V. (2024b). Energy performance of off-grid green cellular base stations. *Perform. Eval.* 165, 102426. doi:10.1016/j.peva.2024.102426

Kuaban, G. S., Gelenbe, E., Czachórski, T., Czekalski, P., and Tangka, J. K. (2023b). Modelling of the energy depletion process and battery depletion attacks for battery-powered internet of things (iot) devices. *Sensors* 23, 6183. doi:10.3390/s23136183

Kuzman, M., del Toro García, X., Escolar, S., Caruso, A., Chessa, S., and López, J. C. (2019). "A testbed and an experimental public dataset for energy-harvested iot solutions," in *2019 IEEE 17th international conference on industrial informatics (INDIN)* (IEEE), 1, 869–876.

Kwiatkowska, M., Norman, G., and Par, D. (2011). "Prism 4.0: verification of probabilistic real-time systems," in *Proc. 23rd international conference on computer aided verification (CAV'11)* (Springer), 6806, 585–591. doi:10.1007/978-3-642-22110-1_47

Lorentzen, L., and Waadeland, H. (1992) *Studies in computation mathematics*, 3. Elsevier.

Massey, W. A., Ekwedike, E., Hempsher, R. C., and Pender, J. J. (2023). A transient symmetry analysis foe the m/m/1/k queue. *Queueing Syst.* 103, 1–43.

Miao, L., Huo, Z.-M., Rong, Y., Mu, H.-W., and Sun, Z.-X. (2023). Iot adaptive threshold energy management algorithm based on energy harvesting. *Ad Hoc Netw.* 149, 103241. doi:10.1016/j.adhoc.2023.103241

Morse, P. (1958). *Queues, inventories and maintenance*. Wiley.

Ng, D. W. K., Lo, E. S., and Schober, R. (2013). Energy-efficient resource allocation in ofdma systems with hybrid energy harvesting base station. *IEEE Trans. Wirel. Commun.* 12, 3412–3427. doi:10.1109/twc.2013.052813.121589

Pecka, P., Nowak, M., Rataj, A., and Nowak, S. (2018). Solving large markov models described with standard programming language. *Commun. Comput. Inf. Sci.* 935, 57–67. doi:10.1007/978-3-030-00840-6_7

Sadatdiynov, K., Cui, L., Zhang, L., Huang, J. Z., Salloum, S., and Mahmud, M. S. (2023). A review of optimization methods for computation offloading in edge computing networks. *Digital Commun. Netw.* 9, 450–461. doi:10.1016/j.dcan.2022.03.003

Sharma, O. P., and Gupta, U. (1982). Transient behaviour of an M/M/1/N queue. *Stoch. Process. Appl.* 13, 327–331. doi:10.1016/0304-4149(82)90019-9

Stehfest, H. (1970). Algorithm 368: numerical inversion of Laplace transforms [D5]. *Commun. ACM* 13, 47–49. doi:10.1145/361953.361969

Tákacs, L. (1962) "Introduction to the theory of queues,". London: Oxford University Press.

Tunc, C., and Akar, N. (2017). Markov fluid queue model of an energy harvesting IoT device with adaptive sensing. *Perform. Eval.* 111, 1–16. doi:10.1016/j.peva.2017.03.004

Varjovi, A. E., and Babaie, S. (2020). Green internet of things (giot): vision, applications and research challenges. *Sustain. Comput. Inf. Syst.* 28, 100448. doi:10.1016/j.suscom.2020.100448

Waadeland, H., and Lorentzen, L. (2008) *Continued fractions*, 1. Springer Science and Business Media.

Wang, H., Li, H., Wang, Z., Chen, X., and Ci, S. (2014). "Stochastic queue modeling and key design metrics analysis for solar energy powered cellular networks," in *2014 international conference on computing, networking and communications (ICNC)* (IEEE), 472–477.